8-13-2015

Fabrication of cellulose fine fiber based membranes embedded with silver nanoparticles via Forcespinning

Fenghua Xu
The University of Texas Rio Grande Valley

Baicheng Weng
The University of Texas Rio Grande Valley

Luis A. Materon
The University of Texas Rio Grande Valley, luis.materon@utrgv.edu

Anxiu Kuang
The University of Texas Rio Grande Valley, anxiu.kuang@utrgv.edu

Jorge A. Trujillo
The University of Texas Rio Grande Valley, jorge.trujillo01@utrgv.edu

See next page for additional authors

Fenghua Xu[a], Baicheng Weng[a], Luis A. Materon, Anxiu Kuang, Jorge A. Trujillo and Karen Lozano*

Fabrication of cellulose fine fiber based membranes embedded with silver nanoparticles via Forcespinning

DOI 10.1515/polyeng-2015-0092
Received March 12, 2015; accepted July 9, 2015; previously published online August 13, 2015

Abstract: This study presents the successful development of cellulose fiber based membranes embedded with silver nanoparticles. These fine fiber membranes were developed utilizing the Forcespinning (FS) technique followed by alkaline hydrolysis treatment. The fiber morphology, homogeneity and yield were optimized by varying spinning parameters such as polymer concentration and angular velocity of the spinnerets. The structure, thermal and mechanical properties, and water absorption capability of the developed membranes were investigated. The cellulose acetate (CA) present in the membrane was converted to cellulose in the presence of embedded silver nanoparticles by alkaline hydrolysis. The silver nanoparticles embedded cellulose membrane exhibits outstanding water absorption capacity with fast uptake rate. Its high porosity, three-dimensional network structure with well-interconnected pores, as well as the intrinsically highly hydrophilic nature of cellulose material greatly favor its potential application as wound dressings. The antimicrobial activity was evaluated by the disk diffusion method. The composite membranes exhibit excellent antimicrobial activity against Gram-negative bacteria *Escherichia coli* and *Pseudomonas aeruginosa*, and Gram-positive *Staphylococcus aureus*, owing to the slow and sustained release of embedded silver nanoparticles.

[a]**Fenghua Xu and Baicheng Weng:** These authors contributed equally to this work.
***Corresponding author: Karen Lozano,** Department of Mechanical Engineering, University of Texas-Pan American, Edinburg, TX 78539, USA, e-mail: lozanok@utpa.edu
Fenghua Xu and Baicheng Weng: Department of Mechanical Engineering, University of Texas-Pan American, Edinburg, TX 78539, USA; and School of Materials Engineering, Yancheng Institute of Technology, Yancheng, Jiangsu 224051, China
Luis A. Materon, Anxiu Kuang and Jorge A. Trujillo: Department of Biology, University of Texas-Pan American, Edinburg, TX 78539, USA

Keywords: antibacterial activity; cellulose; fibers; Forcespinning; silver nanoparticles.

1 Introduction

Nonwoven fine fiber mats possess high porosity, a wide range of pore sizes and large specific surface area [1, 2]. The three-dimensional porous network of these mats is highly favorable for the absorption of the wound exudates, and allows appropriate permeation of oxygen to the wound. More importantly, these fibrous mats are structurally similar to the natural extracellular matrix in skin, therefore providing an optimum scaffold to direct cell growth [3, 4]. Typically, fine fibers are prepared by the electrospinning method, which draws fibers through the use of high-voltage electrostatic forces between an electrically charged polymer solution and a conductive collector [5–7]. In this study, fibers were prepared by the Forcespinning (FS) method, a viable and promising alternative method, which utilizes centrifugal forces to produce fine fibers. This method significantly increases the fiber yield. The productivity at the lab scale has been reported to be higher than 1 g min^{-1} per nozzle (industrial lines are running at tens to hundreds of meters per minute), while that of lab scale electrospinning is typically in the 0.1–0.3 g h^{-1} range [8, 9]. Moreover, given that the conductivity and/or electrostatic charges of the material to be spun into fibers do not play an active role, a broader spectrum of materials, regardless of conductive and non-conductive solutions or melts, can be spun into fibers [9–12].

Cellulose, the most abundant, renewable, biodegradable and biocompatible natural polymer in nature, has drawn considerable attention for a broad spectrum of promising applications. Especially, cellulose is a hydrophilic material, which can effectively absorb wound exudates. More importantly, it can provide a moist environment on a wound, which is favorable for wound healing [13–15]. Cellulose can therefore be applied as suitable wound dressing material for the treatment of large

wounds [16]. However, the hydrogen bond network of cellulose makes it a relatively stable polymer, which does not readily dissolve in typical solvents and lacks a melting point [17]. Hence, it is difficult for cellulose fibers to be directly spun out from a cellulose solution. Herein, cellulose fibers are regenerated by alkaline hydrolysis of spun cellulose acetate (CA) fibers [18–21].

Given that pure cellulose fibers lack antimicrobial activity, silver nanoparticles were incorporated into the spun cellulose fibers. Silver has been well documented to possess a broad spectrum of strong antimicrobial activity [22–24]. Silver ions react strongly with enzymes and proteins which play a vital role in the bacterial respiration and the transport of important substances, resulting in the inactivation of the enzymes and proteins [25]. Moreover, silver ions may bind to the bacterial cell wall, thus disturbing its permeability and inter-membrane exchange [26]. Silver ions may also penetrate inside the cell to interact with phosphorus- and sulfur-containing biomolecules including DNA and proteins, and interact with the ribosome and subsequently inhibit the expression of enzymes and proteins essential to adenosine triphosphate production, which is also believed to one of the major bactericidal actions [27, 28]. In particular, silver nanoparticles with a high specific surface area show higher antimicrobial activity than bulk silver and have been introduced in a variety of materials for applications as antimicrobial wound dressings [15, 24, 25, 29, 30]. Silver nanoparticles slowly convert to silver ions under the physiological system and interact with bacterial cells, keeping silver ions at relatively low levels, therefore avoiding adverse effects on normal cells [15].

In this study, nonwoven cellulose fiber membranes were embedded with silver nanoparticles and mass developed using the FS technique followed by an alkaline hydrolysis treatment. The structure, water absorption capability and thermal properties of the composite membranes were characterized. The antibacterial activity of the developed membranes against Gram-negative bacteria *Escherichia coli* and *Pseudomonas* aeruginosa, and Gram-positive *Staphylococcus aureus* microorganisms was also investigated.

2 Materials and methods

2.1 Materials

CA (M_n=30,000, 39.8 wt% acetyl), dimethyl sulfoxide (DMSO), acetone, ethanol and potassium hydroxide were purchased from Sigma-Aldrich (St. Louis, MO, USA). Silver nanoparticles with sizes of 30–50 nm were obtained from US Research Nanomaterials, Inc (Huston, TX, USA). Anhydrous potassium bromide (>99%) was purchased from Fisher Sci (Pittsburgh, PA, USA). All chemicals were used as received without further purification. Deionized water (DI water, 18 MΩ cm resistance) was produced from Mill-Q (Millipore Ltd., UK).

2.2 Preparation of cellulose-Ag composite fibers

The CA solutions at various concentrations were prepared by dissolving CA in a mixed solution of acetone/DMSO (6:4, v/v) and then allowing the suspension to stir overnight at ambient temperature until it became clear. CA fibers were produced by spinning the as-prepared suspensions on a lab scale spinning system; the Cyclone L-1000M (Fiberio Technology Corporation) was used. The as-prepared polymer suspensions were injected into the cylindrical spinneret equipped with 30 gauge half inch regular bevel needles. The angular velocity of the spinneret forces the polymer solution to elongate through the orifices on the perimeter of the spinneret, therefore releasing the material out, forming fiber jets [9–12]. The spinning was conducted at various rotational speeds to determine optimal processing parameters for the development of fibers. The rotational speeds were varied from 7000 rpm to 9000 rpm. The fibers were collected in a deep dish fiber collector with equally distanced vertical pillars, or deposited on a substrate using a vacuum box to obtain nonwoven fibrous membranes. For the silver nanoparticles embedded CA composite fibers, the nanoparticles (3 wt% to polymer) were dispersed in a mixture of acetone/DMSO (6:4, w/w) by sonication, and then CA was added to the suspension, followed by FS. The prepared composite (CA-Ag) fibers were detached from the collector and dried under vacuum for 24 h at 80°C to remove any traces of solvent.

The membranes were hydrolyzed in a 0.5 M potassium hydroxide ethanol solution at ambient temperature for 3 h to remove the acetyl groups in the precursor CA, and regenerated cellulose-silver composite fibers were obtained. After deacetylation, the membranes were thoroughly rinsed to neutral pH with DI water. The hydrolyzed fibers were then dried under vacuum at 80°C for 24 h.

2.3 Characterizations of fibers

The morphology of the fibers was evaluated using a field-emission scanning electron microscope (FE-SEM; Sigma

VP Carl Zeiss, Germany). The average diameter of the fibers was obtained by measuring more than 100 fibers from randomly selected SEM images using the image analysis software JMicroVision V.1.2.7 (University of Geneva, Geneva, Switzerland). The distribution of silver nanoparticles in the fibers was investigated using scanning transmission electron microscopy (STEM).

Fourier transform infrared spectroscopy (FTIR) measurements were performed on an IFS 55 Equinox FTIR spectrometer (Bruker, Germany). All samples were grinded and mixed with potassium bromide and then pressed to form pellets. The FTIR spectra were recorded in the range of 4000–400 cm^{-1}.

X-ray diffraction (XRD) measurement was carried out on an AXS D8 advance X-ray diffractometer (Bruker, Germany) with a Cu/Kα radiation source filtered with a graphite monochromator (λ=1.5406 Å).

Thermal and mechanical analyses were conducted through differential scanning calorimetry (DSC) using a DSC-Q100 calorimeter and with a dynamic mechanical analyzer (TA Instruments Inc.). Samples of about 10 mg for DSC examination were sealed in aluminum pans and heated from 40°C to 290°C at a heating rate of 5°C min^{-1} under 30 ml min^{-1} of nitrogen flow.

The water absorption capability of the membrane was assessed by immersing the dry membrane in DI water at ambient temperature for 1 h. After 1 h of immersion, the samples were taken out and weighed after removing the surface water with tissue paper. The water uptake capability (%) was calculated as follows: water uptake (%)=$([W\text{-}W_0]/W_0)\times100$, where W_0 and W are the weight of the membrane before and after immersion in water, respectively.

2.4 Release of silver ions

The cellulose-Ag composite membrane was cut into 2.0 cm×2.0 cm pieces. For the *in vitro* release of silver, the samples were immersed in 10 ml of phosphate buffered saline (pH=7.4) at 37°C. The silver concentration in the solution was determined using an inductively coupled plasma optical emission spectrometer (ICP-OES, ICAP-6300, Thermo Fisher, USA).

2.5 Antimicrobial activity assessment

The antimicrobial activity of the developed composite membranes and cellulose membranes was tested against Gram-negative bacteria *E. coli* ATCC 25922 and *P. aeruginosa* ATCC 27853 and Gram-positive *S. aureus* ATCC6538. The test was conducted according to the disk diffusion method [31, 32]. The test organisms were inoculated on agar plates. The fibrous membranes were cut into circular discs with a diameter of 1.2 cm, placed on the plates with sterile forceps and gently pressed to ensure good contact with the solid medium. The plates were then kept in the refrigerators at 5°C for at least 1 h to allow diffusion; afterwards, these were transferred to an incubator at 37°C for 24 h. The zones of growth inhibition around the samples were then measured.

3 Results and discussion

3.1 Morphology and structure of fibers

In the FS technique, the fiber formation and morphology can be greatly influenced by several experimental parameters, such as the polymer concentration and the angular velocity of the spinneret, as reported previously [9–12]. To observe the effect of CA concentration on morphology of the spun fibers, CA solutions in acetone/DMSO mixture with concentrations ranging from 16 wt% to 20 wt% were prepared. No jets were observed on the collector below the concentration of 18 wt%, proven as the minimal concentration required for a suitable and critical polymer chain entanglement that promotes fiber formation. Figure 1 shows SEM images of the spun CA fibers and the corresponding diameter distributions. As presented in Figures 1A and 1D, the fibers obtained at the CA concentration of 18 wt% have a relatively small average fiber diameter of 646 nm, but large beads were formed within the fibers. As the concentration increased to 19 wt% (Figures 1B and 1E) and 20 wt% (Figures 1C and 1F), the beading formation was not observed, however, the average fiber diameter also increased to 1100 nm and 1257 nm, respectively. The results show that the CA concentration has a strong effect on fiber formation and morphology. Moreover, the effect of the angular velocity of the spinneret on CA fiber characteristics was also investigated. Figure 2 shows the SEM images and diameter distributions of the CA fibers at different rotational speeds of 7000 rpm, 8000 rpm and 9000 rpm. It can be observed that increasing the speed from 7000 rpm to 8000 rpm had a negligible effect on the fiber diameter, however, the yield of fibers increased greatly. When the speed was further increased to 9000 rpm, both the yield and average diameter showed a negligible change. Therefore, the optimum spinning parameters for the production of CA fibers were selected to be 19 wt% of

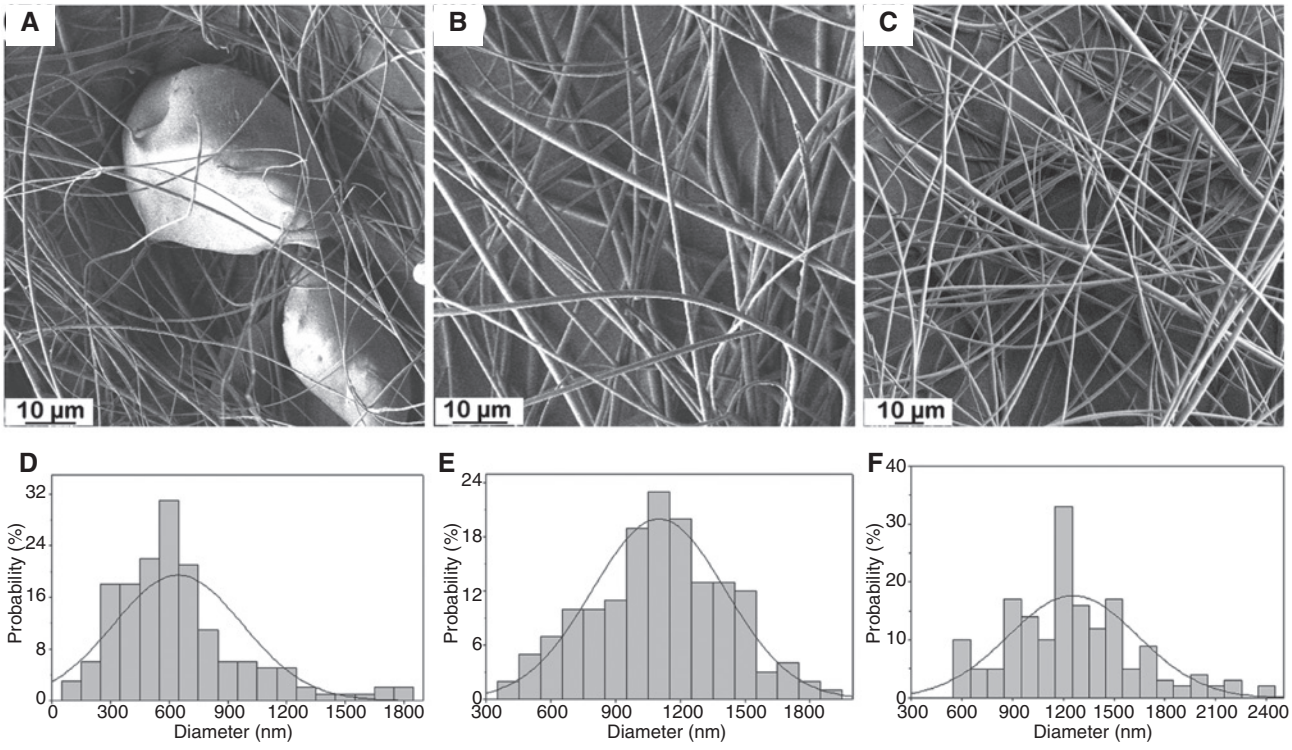

Figure 1: Scanning electron microscopy (SEM) images (A–C) and diameter distributions (D–F) of spun cellulose acetate (CA) fibers at various CA concentrations in an acetone/dimethyl sulfoxide (DMSO) solution: (A, D) 18 wt%, (B, E) 19 wt% and (C, F) 20 wt%.

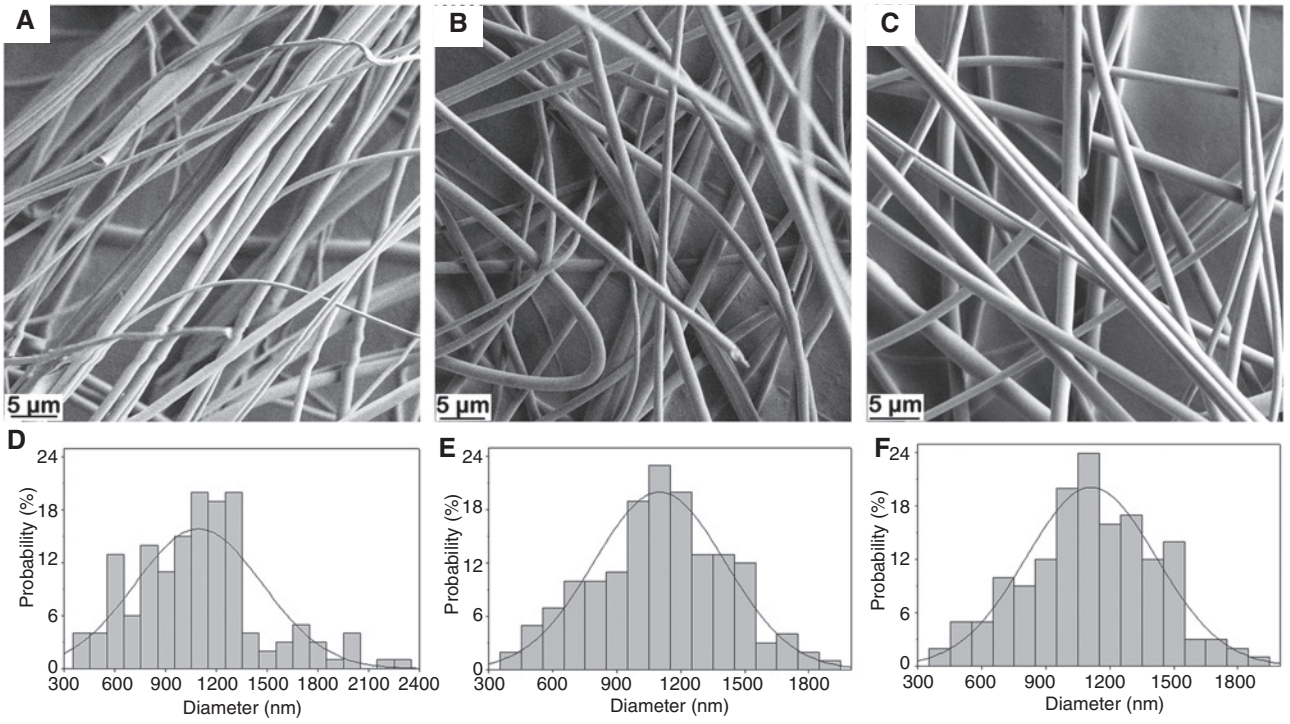

Figure 2: Scanning electron microscopy (SEM) images (A–C) and diameter distributions (D–F) of cellulose acetate (CA) fibers spun from 19 wt% CA suspensions at different rotational speeds: (A, D) 7000 rpm, (B, E) 8000 rpm and (C, F) 9000 rpm.

CA concentration with an angular velocity of 8000 rpm. The composite fibers were obtained by adding the silver nanoparticles into the CA solution. Figures 3A–C show the SEM images of spun fiber based composite membranes and the corresponding diameter distribution. It can be observed that the addition of silver nanoparticles did not affect the homogeneity of the spun fibers. Like pure CA fibers, the produced composite fibers also exhibit a long, beadless and continuous morphology with an average diameter of 1106 nm. Hydrolysis of CA in alkaline solutions has been proved to fully regenerate cellulose by cleavage of the acetyl groups present in the polymer [18, 20, 21]. As such, the silver nanoparticles embedded cellulose composite membrane was prepared by alkaline hydrolysis of the spun composite membrane. Figures 3D–F show SEM images for the obtained composite membrane after deacetylation and the corresponding diameter distribution. It can be observed that after alkaline hydrolysis, the

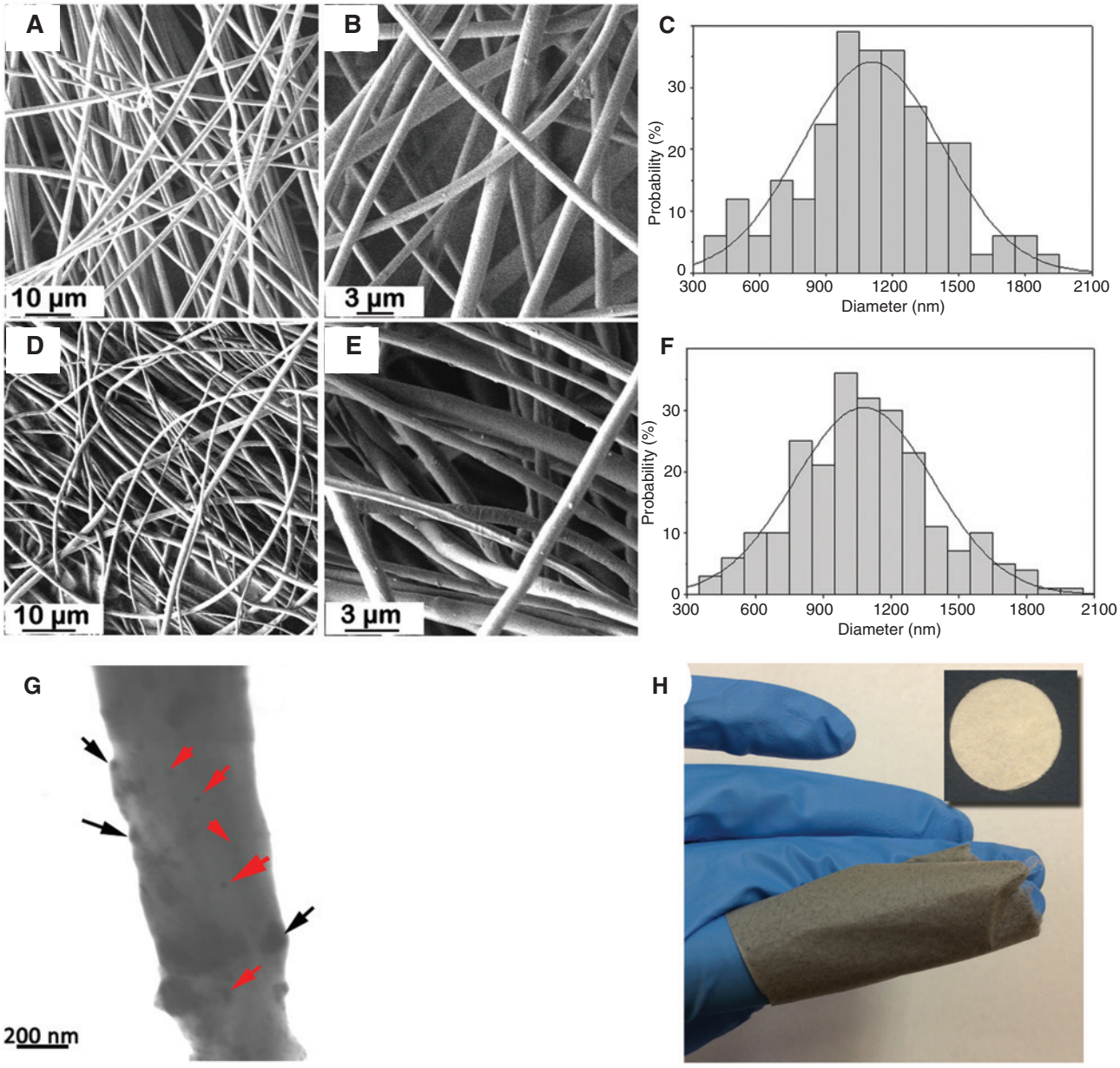

Figure 3: Scanning electron microscopy (SEM) images and diameter distributions of fibrous (A–C) cellulose acetate (CA)-Ag and (D–F) cellulose-Ag composite membranes. (G) Scanning transmission electron microscopy (STEM) images of silver nanoparticles embedded in the cellulose fibers. (H) Picture of a highly conformal and flexible composite membrane. Inserted image in (H) is a photograph of pure cellulose fibrous membrane.

composite fibers show negligible changes in morphology. More importantly, the nonwoven fibrous membrane structure with randomly-oriented, fully-interconnected and highly porous networks remains unchanged, which is consistent with other reports [18, 20, 33]. The distribution of silver nanoparticles in the fibers was studied by STEM. As shown in Figure 3G, silver nanoparticles are not only embedded within the fibers, but also exist on the surfaces, and some aggregates are also observed. The silver nanoparticles on the surfaces are believed to play a more important role in the antimicrobial activity. Figure 3H shows the photograph of the as-obtained nonwoven composite membrane; with the incorporation of silver nanoparticles, the membrane became gray. The composite membranes were shown to be highly conformal and flexible, thus suitable for irregular and intricate wounds.

FTIR spectroscopy was employed to analyze the change in chemical structure of the spun composite fibers after deacetylation and to confirm the full hydrolysis of fiber composite membranes into cellulose-Ag composite membranes. Figure 4 shows the FTIR spectra of spun CA fibers and composite fibers before and after deacetylation. The spectrum of the composite fibers shows the typical absorption features of CA polymer. The strong characteristic adsorption peaks at 1745 ($\nu_{C=O}$), 1375 ($\nu_{C\text{-}CH_3}$), and 1235 cm^{-1} ($\nu_{C\text{-}O\text{-}C}$), corresponding to the vibrations of the acetate group were observed, and the wide stretching band at 3500 cm^{-1} can be ascribed to the hydroxyl groups ($\nu_{O\text{-}H}$) of CA polymer. With the incorporation of silver nanoparticles, the hydroxyl vibration peak at 3500 cm^{-1} slightly decreases. After deacetylation, the peaks attributed to the vibrations of the acetate group disappear, while the intensity of the absorption peak for $\nu_{O\text{-}H}$ increases and shifts to 3400 cm^{-1} [19, 20, 33–35]. These results suggest that acetyl groups of CA in the composite were fully converted to hydroxyl groups and thus cellulose was completely regenerated after alkaline hydrolysis. In addition, the weak adsorption peak at 540 cm^{-1}, corresponding to Ag-O, shows the incorporation of silver nanoparticles in the fibers.

Figure 5 shows XRD patterns of fibrous membranes of CA, CA-Ag and cellulose-Ag. The XRD pattern of CA membrane exhibits a broad peak around 21°, indicating an amorphous structure for the spun CA fibers. With the incorporation of silver nanoparticles, the diffraction peak shifts to around 17.5°, the relative peak intensity shows a slight increase and another broad peak posited around 8° is observed. Four more peaks are also observed at 38°, 44°, 64.5° and 77° corresponding to (111), (200), (220) and (311) planes, respectively, of the face centered cubic structure of the metallic silver nanoparticles [15, 36]. These results confirm the successful incorporation of silver nanoparticles in the CA fibers, and indicate that the silver nanoparticles are actively interacting with the CA microstructure acting as nuclei sites during the spinning process to induce CA crystallization. After deacetylation, the composite membrane exhibits two diffraction peaks at 2θ values of 12°and 20.5°, resembling the typical diffraction pattern of cellulose II [37], while the peaks of CA disappeared, therefore confirming the results obtained from the FTIR studies. Moreover, it also exhibits four characteristic

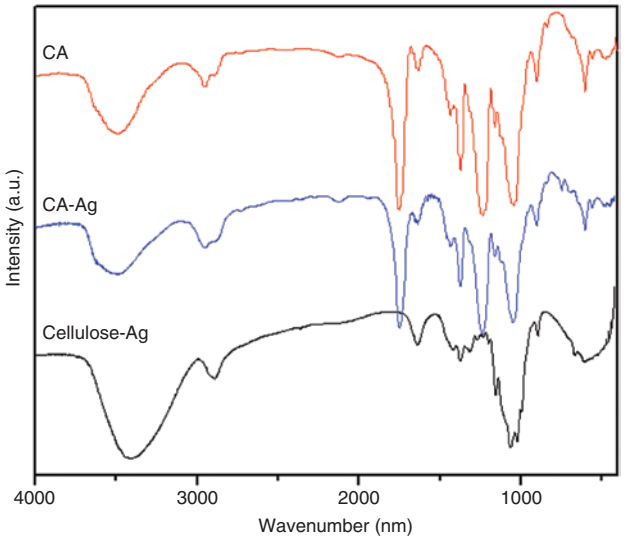

Figure 4: Fourier transform infrared spectroscopy (FTIR) spectra of pure cellulose acetate (CA) fibers, CA-Ag composite fibers and cellulose-Ag composite fibers.

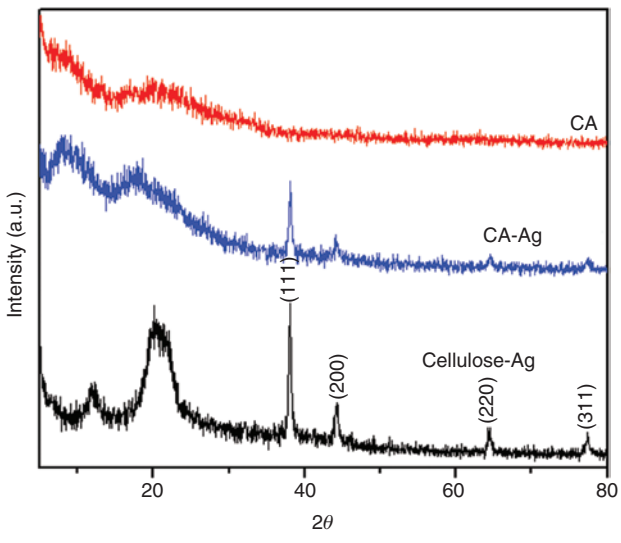

Figure 5: X-ray diffraction (XRD) patterns of pure cellulose acetate (CA) fibers, CA-Ag composite fibers and cellulose-Ag composite fibers.

peaks of silver nanoparticles. These results indicate that CA matrix in the composite was completely deacetylated to cellulose in the presence of added silver nanoparticles, and thus cellulose-Ag composite fibers were successfully obtained.

DSC analyses were performed to investigate the thermal behavior of the spun fibrous membranes. As shown in Figure 6, the CA fibers and the CA-Ag composite fibers show similar behavior. The glass transition temperature attributed to CA is observed at 204.5°C for both systems. An endotherm centered at 227.8°C, which corresponds to the melting temperature of CA, is also observed for both systems and is well in agreement with previous reports [18, 20, 33]. The results show that the incorporation of a low amount of silver nanoparticles did not affect the thermodynamic phase transitions. Moreover, in the case of pure CA fibers, a broad endothermic peak is observed in the temperature range of 40–95°C with a maximum at 62°C and ascribed to loss of absorbed water molecules. In contrast, with the incorporation of silver nanoparticles, the endothermic peak is shifted to the temperature range of 40–100°C with a maximum at 67°C, which may be due to the strong interaction between silver and H_2O molecules. After alkaline hydrolysis treatment of the composite fibers, both the melting temperature and the glass transition temperature disappeared. The dehydration peak due to loss of water molecules is further upshifted to the temperature range of 40–150°C centering at 80°C and becomes stronger, owing to the stronger interaction between the regenerated cellulose with higher hydrophilicity and the bounded water molecules [33, 38–40]. The results further show that acetyl groups in the CA fibers were fully hydrolyzed to hydroxyl groups by alkaline hydrolysis, and as a consequence, the regenerated cellulose-Ag composite membranes absorb water more strongly.

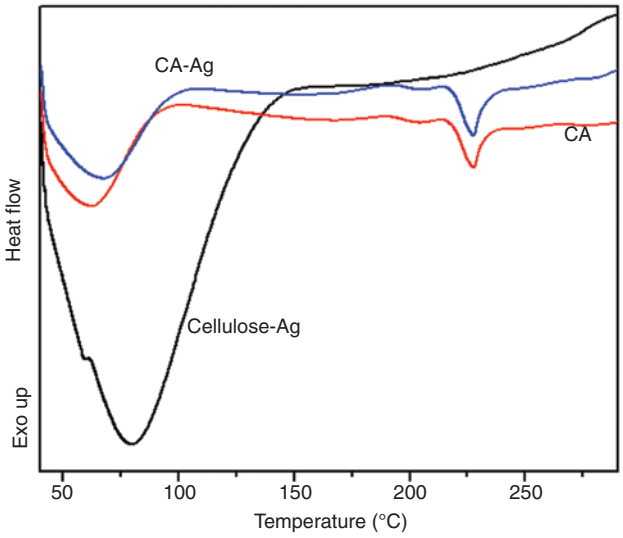

Figure 6: Differential scanning calorimetry (DSC) curves of pure cellulose acetate (CA) fibers, CA-Ag composite fibers and cellulose-Ag composite fibers.

Typical stress-strain curves of fibrous membranes of CA, cellulose and cellulose-Ag are presented in Figure 7A. After deacetylation, the tensile strength of the membrane increases from 20 MPa to 33 MPa, coupled with a reduction in strain at break, indicating a decrease in toughness and flexibility [12]. With the incorporation of Ag nanoparticles, the tensile strength slightly increases to 35 MPa.

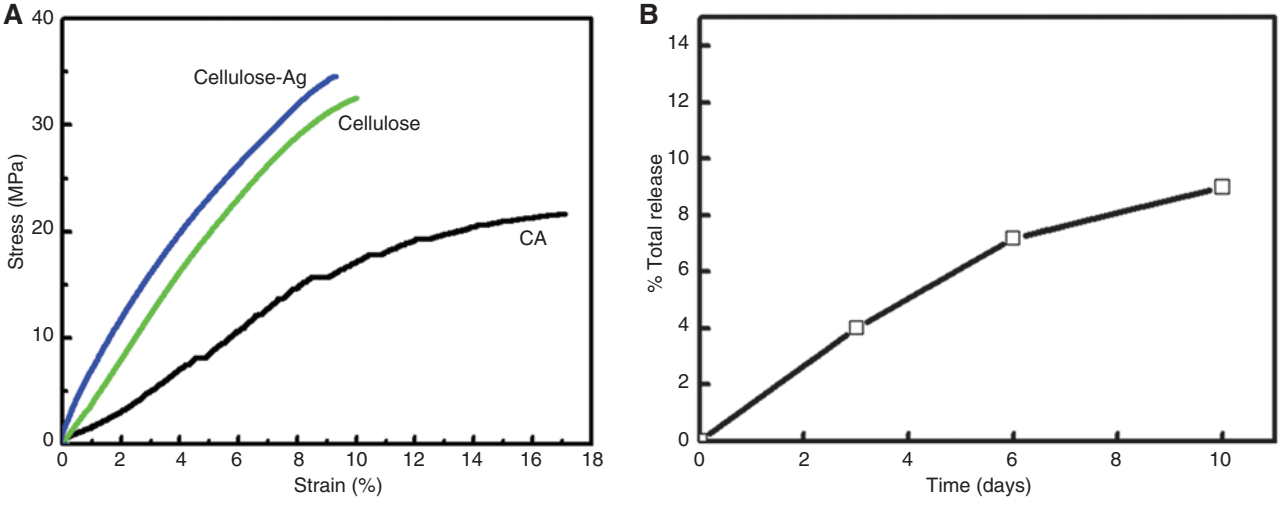

Figure 7: (A) Tensile strength curves of fibrous membranes of cellulose acetate (CA), cellulose and cellulose-Ag. (B) Silver ion release curve of fibrous cellulose-Ag composite membrane in phosphate buffered saline (PBS) (pH=7.4).

For a simple composite system without micromechanical interlocking and chemical bonding between the filler and matrix, the load transfer from the matrix to filler is realized through a weak bonding between the filler and the matrix [12]. For the cellulose-Ag composite, the load may be transferred from Ag to cellulose by hydrogen bonding between Ag-OH/Ag-O and the hydroxyl bonds of cellulose. Therefore, the tensile strength of the obtained fibers increases with incorporation of silver nanoparticles into the fibers.

3.2 Water absorption capability of the membrane

The desirable wound dressing must absorb excess exudates without leakage to its surface [2]. Therefore, the water absorption capability of the cellulose-Ag composite membrane was analyzed by soaking the membrane in water at room temperature for 1 h. Its water absorption capability was increased to 310%, which is higher than that of the CA-Ag membrane (260%). In particular, it was observed that the composite membrane exhibited a rapid water uptake rate. Most importantly, it is worth mentioning that the composite membrane also shows high water retention capability, which can provide a prolonged moist microenvironment on the wound benefitting the re-epithelialization of the wound and preventing the formation of a scab [13, 14]. The cellulose-Ag composite membrane exhibits high porosity, well-interconnected microporous three-dimensional network structure and a large specific surface area, as well as the high intrinsic hydrophilicity of cellulose material, leading to easier penetration and absorption and higher retention of water. Therefore, the as-produced cellulose-Ag composite membranes are shown to have the absorption characteristics needed for application as wound dressing materials.

3.3 Release of silver ions

The silver ions release behavior of fibrous cellulose-Ag composite membrane is shown in Figure 7B. The silver

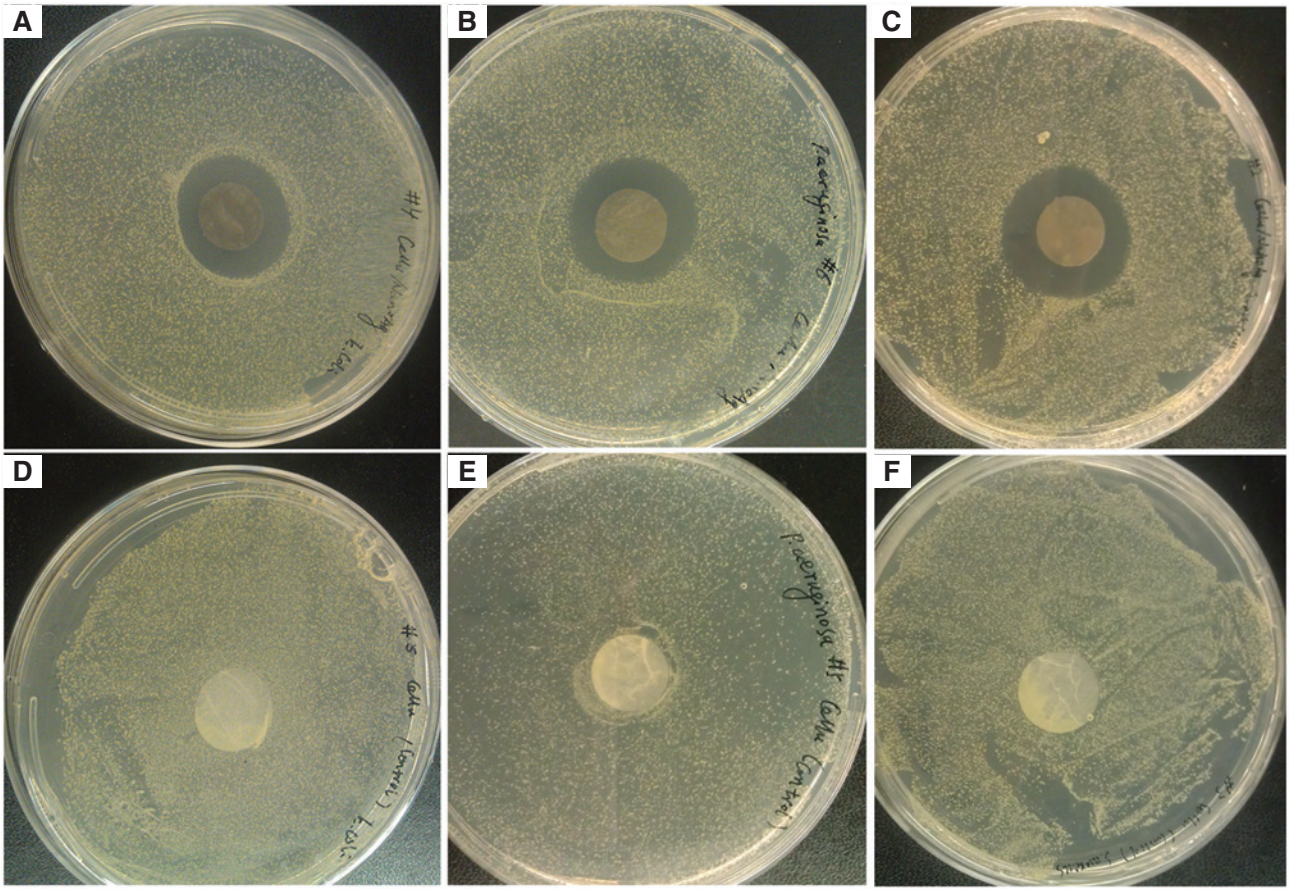

Figure 8: Antimicrobial activity of (A–C) nonwoven silver nanoparticles-embedded cellulose composite membranes and (D–F) pure cellulose membranes against (A, D) *Escherichia coli*, (B, E) *Pseudomonas aeruginosa* and (C, F) *Staphylococcus aureus*.

ions were released slowly and steadily along with incubation time. The silver nanoparticles on the surface of fibers were firstly released, whereas the nanoparticles inside diffused to the outside gradually, resulting in a sustained release of silver which can inhibit the growth of bacteria in a long-term manner; the silver ions will not be so high enough to adversely affect normal cells [15, 28, 41].

3.4 Antimicrobial activity assessment

The ideal dressings should protect the wound against microbial contamination. Herein, to evaluate the effect of the fiber based membranes against bacterial growth, Gram-negative bacteria *E. coli* and *P. aeruginosa*, and Gram-positive *S. aureus* microorganisms which are often found on infected wounds were used. The antibacterial activity was measured by the disk diffusion method. Figure 8 shows the antibacterial assessment of the nonwoven fiber cellulose-Ag composite membranes on the growth inhibition of *E. coli*, *P. aeruginosa* and *S. aureus*. For comparison, results for pure cellulose membranes are also presented. It can be observed that the cellulose-Ag composite membranes exhibit clear zones of growth inhibition, showing significant antimicrobial activity against all three bacterial strains. In the case of the pure cellulose, no zones of growth inhibition were observed around the membranes, indicating that the as-obtained fibrous pure cellulose membranes have no activity against bacteria. Specifically, the zones of growth inhibition were 5–7 mm (Figure 8). The results indicate that the silver nanoparticles embedded inside endow the cellulose composite fibers with an effective antimicrobial activity. The silver nanoparticles on the surface of fibers are easily released while the nanoparticles inside diffuse to the outside gradually providing a sustained release of silver, resulting in a long-term effective antibacterial activity [28]. Silver nanoparticles are also slowly converted to silver ions under the physiological system and interact with bacterial cells, thus silver ions will not be so high enough to adversely affect normal cells [15].

4 Conclusion

Nonwoven fiber membranes made of cellulose embedded with silver nanoparticles were successfully developed by alkaline hydrolysis of CA-Ag membranes. The fibrous CA-Ag membranes were mass produced using the FS technique. The optimum concentration for the spinning of CA suspensions was found to be 19 wt% in a solution of acetone/DMSO (6:4, w/w). Fiber membranes were spun at a rotational speed of 8000 rpm. CA-Ag composite membranes were obtained by incorporating 0.3 wt% of silver nanoparticles. FTIR, XRD and DSC analyses confirm that the CA in the composite membrane was completely deacetylated to cellulose by alkaline hydrolysis in the presence of silver nanoparticles. The resulting composite fibers are observed to be long, beadless and continuous. STEM analysis show silver nanoparticles distributed in the fibers with some level of aggregation. The obtained cellulose-Ag composite membranes showed a nonwoven three-dimensional network, with superior water absorption capacity of 310%, with a rapid uptake rate and high water retention capability. It was observed that the cellulose-Ag composite membranes exhibit apparent zones of growth inhibition, suggesting their significant antimicrobial activity against Gram-negative bacteria *E. coli* and *P. aeruginosa* and Gram-positive *S. aureus*, whereas pure cellulose membranes exhibit no antimicrobial activity. The developed antimicrobial fiber based composite membranes resembling the extracellular matrix in skin show potential for applications as wound dressing materials.

Acknowledgments: This work was financially supported by the National Science Foundation under DMR grant #0934157.

Conflict of interest statement: Dr. Lozano and the University of Texas-Pan American have research related financial interests with Fiberio Technology Corporation.

References

[1] Bhattarai SR, Bhattarai N, Yi HK, Hwang PH, Cha DI, Kim HY. *Biomaterials* 2004, 25, 2595–2602.
[2] Zahedi P, Rezaeian I, Ranaei-Siadat SO, Jafari SH, Supaphol P. *Polym. Adv. Technol.* 2010, 21, 77–95.
[3] Pham QP, Sharma U, Mikos AG. *Tissue Eng.* 2006, 12, 1197–1211.
[4] Khanam N, Mikoryak C, Draper RK, Balkus KJ Jr. *Acta Biomater.* 2007, 3, 1050–1059.
[5] Li D, Xia Y. *Adv. Mater.* 2004, 16, 1151–1170.
[6] Paneva D, Bougard F, Manolova N, Dubois P, Rashkov I. *Eur. Polym. J.* 2008, 44, 566–578.
[7] Saiyasombat C, Maensiri S. *J. Polym. Eng.* 2008, 28, 5–18.
[8] Ramakrishna S. *An Introduction to Electrospinning and Nanofibers Technology*, World Scientific Publishing Co.: Singapore, 2005, p. 130.
[9] Sarkar K, Gomez C, Zambrano S, Ramirez M, Hoyos E, Vasquez H, Lozano K. *Mater. Today* 2010, 13, 12–14.
[10] Weng B, Xu F, Garza G, Alcoutlabi M, Salinas A, Lozano K. *Polym. Eng. Sci.* 2014, 55, 81–87.

[11] Weng B, Xu F, Lozano K. *J. Appl. Polym. Sci*. 2014, 131, 40302.
[12] Weng B, Xu F, Salinas A, Lozano K. *Carbon* 2014, 75, 217–226.
[13] Li H, Yang J, Hu X, Liang J, Fan Y, Zhang X. *J. Biomed. Mater. Res. A* 2011, 98A, 31–39.
[14] Winter GD. *Nature* 1962, 193, 293–294.
[15] Maneerung T, Tokura S, Rujiravanit R. *Carbohydr. Polym*. 2008, 72, 43–51.
[16] Czaja W, Krystynowicz A, Bielecki S, Brown RM Jr. *Biomaterials* 2006, 27, 145–151.
[17] Kroonbatenburg LMJ, Kroon J, Northolt MG. *Polym. Commun.* 1986, 27, 290–292.
[18] Liu H, Hsieh Y. *J. Polym. Sci., Part B: Polym. Phys.* 2002, 40, 2119–2129.
[19] Son WK, Youk JH, Lee TS, Park WH. *J. Polym. Sci., Part B: Polym. Phys.* 2004, 42, 5–11.
[20] Vallejos ME, Peresin MS, Rojas OJ. *J. Polym. Environ.* 2012, 20, 1075–1083.
[21] Han SO, Youk JH, Min KD, Kang YO, Park WH. *Mater. Lett.* 2008, 62, 759–762.
[22] Nowack B, Krug HF, Height M. *Environ. Sci. Technol.* 2011, 45, 1177–1183.
[23] Su YH, Yin ZF, Xin HL, Zhang HQ, Sheng JY, Yang YL, Du J, Ling CQ. *Int. J. Nanomed.* 2011, 6, 1579–1586.
[24] Abdelgawad AM, Hudson SM, Rojas OJ. *Carbohydr. Polym.* 2014, 100, 166–178.
[25] Cho KH, Park JE, Osaka T, Park SG. *Electrochim. Acta* 2005, 51, 956–960.
[26] Percival SL, Bowler PG, Russell D. *J. Hosp. Infect.* 2005, 60, 1–7.
[27] Yamanaka M, Hara K, Kudo J. *Appl. Environ. Microbiol.* 2005, 71, 7589–7593.
[28] Yuan J, Geng J, Xing Z, Shen J, Kang IK, Byun H. *J. Appl.* Polym. Sci. 2010, 116, 668–672.
[29] Choi O, Deng KK, Kim NJ, Ross L Jr, Surampalli RY, Hu Z. *Water Res.* 2008, 42, 3066–3074.
[30] Rujitanaroj P, Pimpha N, Supaphol P. *Polymer* 2008, 49, 4723–4732.
[31] Bauer RW, Kirby MDK, Sherris JC, Turck M. *Am. J. Clin. Pathol.* 1996, 45, 493–496.
[32] Unnithan AR, Barakat NAM, Tirupathi Pichiah PB, Gnanasekaran G, Nirmala R, Cha YS, Jung CH, El-Newehy M, Kim HY. *Carbohydr. Polym.* 2012, 90, 1786–1793.
[33] Ma Z, Kotaki M, Ramakrishna S. *J. Membr. Sci.* 2005, 265, 115–123.
[34] Deng H, Zhou X, Wang X, Zhang C, Ding B, Zhang Q, Du Y. *Carbohydr. Polym.* 2010, 80, 474–479.
[35] Son WK, Youk JH, Park WH. *Biomacromolecules* 2004, 5, 197–201.
[36] Jiang GH, Wang L, Chen T, Yu HJ, Wang JJ. *J. Mater. Sci.* 2005, 40, 1681–1683.
[37] Azubuike CP, Okhamafe AO. *Int. J. Recycling Org. Waste Agric.* 2012, 1, 1–9.
[38] Bertran MS, Dale BE. *J. Appl. Polym. Sci.* 1986, 32, 4241–4253.
[39] Ford JL. *Int. J. Pharm.* 1999, 179, 209–228.
[40] Szczeœniak L, Rachocki A, Tritt-Goc J. *Cellulose* 2008, 15, 445–451.
[41] Breitwieser D, Moghaddam MM, Spirk S, Baghbanzadeh M, Pivec T, Fasl H, Ribitsch V, Kappe CO. *Carbohydr. Polym.* 2013, 94, 677–686.